doi:10.1016/j.jmb.2008.11.003 J. Mol. Biol. (2009) 385, 393–404

JMB

Available online at www.sciencedirect.com

ScienceDirect

ELSEVIER

Role of Allosteric Switch Residue Histidine 195 in Maintaining Active-Site Asymmetry in Presynaptic Filaments of Bacteriophage T4 UvsX Recombinase

Joshua N. Farb and Scott W. Morrical*

Departments of Biochemistry, and Microbiology and Molecular Genetics, and Vermont Cancer Center, University of Vermont College of Medicine, Burlington, VT 05405, USA

Received 8 September 2008; received in revised form 30 October 2008; accepted 3 November 2008
Available online
12 November 2008

Recombinases of the highly conserved RecA/Rad51 family play central roles in homologous recombination and DNA double-stranded break repair. RecA/Rad51 enzymes form presynaptic filaments on single-stranded DNA (ssDNA) that are allosterically activated to catalyze ATPase and DNA strand-exchange reactions. Information is conveyed between DNA- and ATP-binding sites, in part, by a highly conserved glutamine residue (Gln194 in *Escherichia coli* RecA) that acts as an allosteric switch. The T4 UvsX protein is a divergent RecA ortholog and contains histidine (His195) in place of glutamine at the allosteric switch position. UvsX and RecA catalyze similar strand-exchange reactions, but differ in other properties. UvsX produces both ADP and AMP as products of its ssDNA-dependent ATPase activity—a property that is unique among characterized recombinases. Details of the kinetics of ssDNA-dependent ATP hydrolysis reactions indicate that UvsX-ssDNA presynaptic filaments are asymmetric and contain two classes of ATPase active sites: one that generates ADP, and another that generates AMP. Active-site asymmetry is reduced by mutations at the His195 position, since UvsX-H195Q and UvsX-H195A mutants both exhibit stronger ssDNA-dependent ATPase activity, with lower cooperativity and markedly higher ADP/AMP product ratios, than wild-type UvsX. Reduced active-site asymmetry correlates strongly with reduced ssDNA-binding affinity and DNA strand-exchange activity in both H195Q and H195A mutants. These and other results support a model in which allosteric switch residue His195 controls the formation of an asymmetric conformation of UvsX-ssDNA filaments that is active in DNA strand exchange. The implications of our findings for UvsX recombination functions, and for RecA functions in general, are discussed.

Keywords: recombination; presynaptic filament; ATPase; kinetics; strand exchange

Edited by J. Karn

Introduction

Homologous recombination is an essential part of life and is important in heredity and evolution, as well as in the maintenance of genomic stability.[1,2] Enzymes of the highly conserved RecA recombinase family catalyze DNA strand-exchange reactions that are central to the mechanisms of homologous recombination and recombinational DNA repair. Valuable information on recombination mechanisms has come through studies of the bacteriophage T4 recombination system and UvsX recombinase, the T4 RecA ortholog. UvsX plays central roles in phage recombination, recombination-dependent DNA replication, and double-stranded break repair pathways.[3–5]

Although relatively divergent in sequence, UvsX shares many properties in common with other well-characterized recombinases such as *Escherichia coli* RecA (EcRecA) and *Saccharomyces cerevisiae* Rad51 (ScRad51) proteins, including the ability to catalyze DNA strand exchanges between homologous single-

**Corresponding author.* E-mail address: smorrica@uvm.edu.

Abbreviations used: ssDNA, single-stranded DNA; EcRecA, *Escherichia coli* RecA; ScRad51, *Saccharomyces cerevisiae* Rad51; dsDNA, double-stranded DNA; RFIII, replicative fragment III; TLC, thin-layer chromatography; PP_i, inorganic pyrophosphate; P_i, inorganic phosphate; EDTA, ethylenediaminetetraacetic acid; NCBI, National Center for Biotechnology Information; PDB, Protein Data Bank.

stranded DNA (ssDNA) and double-stranded DNA (dsDNA) molecules, and the ability to catalyze ssDNA-dependent ATP hydrolysis.[2,3] These activities require the formation of a presynaptic filament consisting of recombinase bound cooperatively to ssDNA. Despite these overall similarities, UvsX exhibits interesting differences in activity compared to other recombinases. Most notably, UvsX generates both ADP and AMP as products of its nucleotidase activity—a property that is unique among characterized recombinases.[6] UvsX also exhibits distinctive sequence characteristics within the highly conserved RecA catalytic core domain, including the substitution of histidine for glutamine at a key allosteric switch position.[7]

The original crystal structure of EcRecA[8] inferred the importance of the side chain of residue Gln194 in detecting the γ-phosphate of ATP bound to the P-loop region of the enzyme active site. Subsequent structures of EcRecA and orthologs from *Mycobacterium smegmatis*, *Mycobacterium tuberculosis*, *Deinococcus radiodurans*, *Methanococcus voltae*, and *Thermococcus kodakaraensis* confirm that this highly conserved glutamine residue plays an important role in sensing the γ-phosphate of bound nucleoside triphosphate.[9–16] It is also clear from these and other studies that Gln194 is positioned at the base of the DNA-binding loop L2, which is the primary site involved in protein–ssDNA interactions.[17–19] In the structure of an EcRecA derivative bound to ssDNA, the side chain of Gln194 forms part of a hydrogen-bonding network linking γ-phosphate to L2 and ssDNA.[15] Thus, Gln194 is well-positioned to coordinate allosteric communications between nucleotide- and polynucleotide-binding sites. Data indicate that EcRecA is intolerant of all substitutions at the Gln194 position, since all mutants are defective in recombination and LexA repressor cleavage *in vivo*.[17] Biochemical analyses of EcRecA-Q194N, EcRecA-Q194E, and EcRecA-Q194A mutants indicate that all retain basal ssDNA- and ATP-binding activities; however, ssDNA fails to stimulate the basal ATPase activity of EcRecA, and the enzyme fails to enter a high-affinity ssDNA-binding state in response to ATP binding.[17–19] Available data indicate that Gln194 controls allosteric switching between the ATP-induced high-affinity ssDNA-binding state associated with homologous pairing activity and an ADP-induced low-affinity ssDNA-binding state associated with presynaptic filament dissociation.[2,17–20]

Sequence alignments and comparisons to known RecA structures indicate that, in UvsX protein, His195 occupies the same structural niche as Gln194 in EcRecA, so that this histidine residue in UvsX potentially represents a conservatively substituted allosteric switch residue.[7] To study the importance of this residue in controlling the catalytic properties of UvsX protein, we carried out studies of the DNA strand-exchange and ATPase activities of wild-type UvsX in comparison with conservative H195Q and nonconservative H195A mutants. Both mutants exhibit defects in DNA strand-exchange reactions consistent with decreased ssDNA-binding affinity. Nevertheless, UvsX tolerates conservative substitution at the His195 locus, since the H195Q mutant retains weak DNA strand-exchange activity that is stimulated by the phage ssDNA-binding protein Gp32. Kinetic properties of H195Q and H195A mutants exhibit unexpected and striking differences from wild-type UvsX, including higher ssDNA-dependent ATPase activity, increased ADP/AMP product ratio, and lower cooperativity for substrates. The data indicate that His195 plays an important role in establishing asymmetry within the presynaptic filament between active sites that generate ADP as product and those that generate AMP. Mutations at this locus reduce active-site asymmetry, which correlates strongly with a reduced affinity for ssDNA and with reduced DNA strand-exchange activity. Our studies reveal new details of the allosteric mechanism of UvsX recombinase and have implications for the functioning of other RecA/Rad51 orthologs as well.

Results

Sequence alignments of UvsX protein and the RecA family

Figure 1 displays amino acid sequence alignments of UvsX enzymes from T-even bacteriophages, in comparison with other RecA family enzymes from diverse bacterial, eukaryotic, and archaeal organisms. The sequences shown span a segment of the strongly conserved catalytic core region of the RecA family surrounding DNA-binding loops L1 and L2. The T4 UvsX His195 residue corresponds to the allosteric switch residue Gln194 in EcRecA.[7,17] This residue is widely conserved as glutamine throughout the bacterial, eukaryotic, and archaeal kingdoms, but is replaced by histidine in the UvsX subfamily (Fig. 1). The UvsX sequences shown in Fig. 1 are from representative T-even bacteriophages of diverse host ranges, including cyanophages. Interestingly, histidine also replaces glutamine at the corresponding position in the Dmc1 recombinase of the parasitic protist *Theileria parva*. Note that, in all sequences, the Gln/His switch residue immediately precedes the sequence-divergent DNA-binding loop L2, which contains the primary DNA-binding site.[17–19]

Effects of His195 missense mutations on UvsX DNA strand-exchange activity

UvsX residue His195 was mutated to glutamine as a potentially conservative change mimicking the active-site configuration of cellular RecA orthologs. A histidine-to-alanine mutation was also introduced at this locus as a potential functional knockout. Figure 2 compares the DNA strand-exchange activities of wild-type UvsX to those of the H195Q and H195A mutants. Previous studies showed that, at relatively high concentrations, wild-type UvsX protein catalyzes DNA strand exchange between homologous

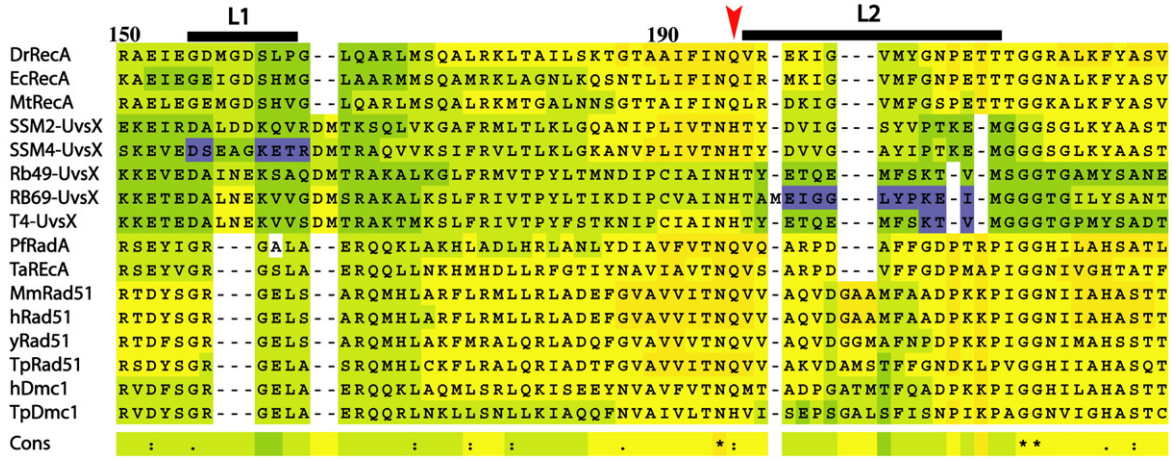

Fig. 1. Partial sequence alignment of selected members of the RecA protein family using Tcoffee algorithm.[44] Sequences from the RecA core domain surrounding DNA-binding loops L1 and L2 are depicted. The residue numbering scheme is based on the bacteriophage T4 UvsX protein sequence. Aligned protein sequences include the following: *D. radiodurans* RecA (DrRecA), *M. tuberculosis* RecA (MtRecA), *E. coli* RecA (EcRecA), cyanophage P-SSM2 and P-SSM4 UvsX (P-SSM2-UvsX and P-SSM4-UvsX), enterobacteria phage RB49 and RB69 UvsX (RB49-UvsX and RB69-UvsX), bacteriophage T4 UvsX (T4-UvsX), *P. furiosus* RadA (PfRadA), *Ther. acidophilum* RecA (TaRecA), *Mu. musculus* Rad51 (MmRad51), human Rad51 (hRad51), *S. cerevisiae* Rad51 (yRad51), *T. parva* strain Muguga Rad51 (TpRad51), human Dmc1 (hDmc1), and *T. parva* strain Muguga Dmc1 (TpDmc1). The color scheme is an indicator of the reliability of the alignment for each residue in every sequence, from the least reliable (blue) to the most reliable (red). Within the consensus sequence, absolutely, strongly, and moderately conserved residues are denoted with an asterisk, two dots, and one dot, respectively. DNA-binding loops L1 (EcRecA residues 157–164) and L2 (EcRecA residues 195–209) are denoted by black bars above the sequence. The location of the γ-phosphate sensor/allosteric switch residue Gln194 in EcRecA (His195 in T4-UvsX) is denoted by a red arrow.

ssDNA and dsDNA molecules in the absence of other protein factors such as Gp32 (T4 ssDNA-binding protein) and UvsY (T4 recombination mediator protein).[21–23] We tested the intrinsic DNA strand-exchange activities of UvsX wild-type, H195A, and H195Q enzymes under similar conditions, with the results shown in Fig. 2a. At a concentration of 6 μM (a 2.4-fold excess over ssDNA-binding sites, assuming that $n=4$ nucleotide residues/protomer[24]), wild-type UvsX readily promotes DNA strand exchange in the absence of other protein factors, as seen by the time-dependent decrease in labeled linear dsDNA substrate and the corresponding appearance of labeled joint molecules and aggregates (Fig. 2a). These aggregates are a characteristic product of UvsX-catalyzed strand exchange, which generates branched networks of DNA caused by multiple synapsis events per DNA molecule.[21,25,26] Otherwise identical reactions containing UvsX-H195A showed no DNA strand-exchange activity, whereas reactions containing UvsX-H195Q showed weak DNA strand-exchange activity, as evidenced by the appearance of DNA aggregates at late time points (Fig. 2a).

At lower enzyme concentrations, the DNA strand-exchange activity of wild-type UvsX is stimulated strongly by Gp32, the T4 ssDNA-binding protein.[21–23] Figure 2b shows strand-exchange reactions performed with either wild-type, H195A, or H195Q UvsX at a concentration of 3 μM (a 1.2-fold excess over ssDNA-binding sites), all in the presence of 1.43 μM Gp32 (exactly saturating with respect to ssDNA-binding sites, assuming that $n=7$ nucleotide residues/protomer[27,28]). Under these conditions, the reaction with wild-type UvsX was very robust, with nearly all replicative fragment III (RFIII; linearized M13mp18 dsDNA) substrates converted into high-molecular-weight branched DNA products by the 2-min time point (Fig. 2b). UvsX-H195A again showed no activity, demonstrating that Gp32 apparently cannot rescue the strand-exchange defect of this mutant. In contrast, UvsX-H195Q exhibited a moderate level of strand-exchange activity in the presence of Gp32, with intermediates appearing as early as the 2-min time point (Fig. 2b).

Effects of His195 missense mutations on UvsX-ssDNA-binding activity

The basal ATP-independent ssDNA-binding activities of wild-type and mutant UvsX proteins were compared at equilibrium using a fluorescent OliGreen dye-displacement assay (Fig. 3). Wild-type UvsX binds tightly to ssDNA at this salt concentration (50 mM NaCl), yielding a binding curve with a sharp end point corresponding to a binding site size of four nucleotide residues per UvsX monomer (Fig. 3), consistent with previous results.[24] The basal ssDNA-binding activities of H195Q and H195A mutants are similar to each other, but much weaker than that of wild type, since large excesses of either mutant protein over ssDNA are required to approach complete displacement of the OliGreen dye from ssDNA (Fig. 3). The weaker basal ssDNA-binding activities of these mutants may be at least partially responsible for their defects in DNA strand exchange.

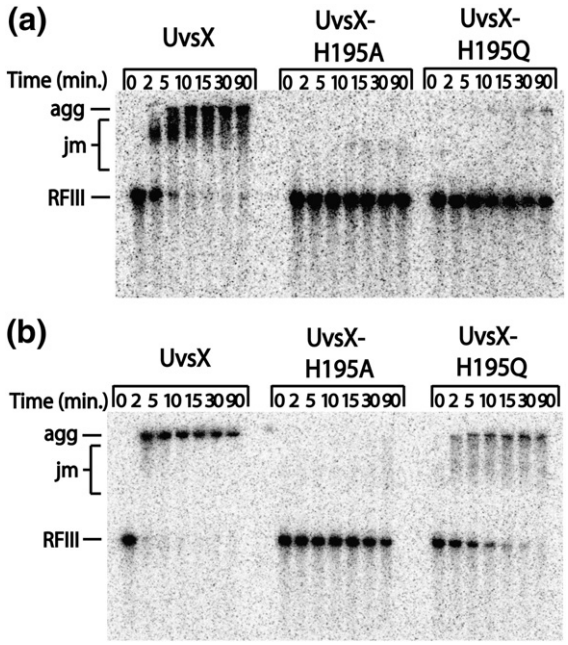

Fig. 2. DNA strand-exchange activities of UvsX wild-type and missense mutants. Experiments were carried out as described in Materials and Methods. Time points of the reactions are shown immediately above the gel. DNA aggregates (agg) are branched networks of dsDNA and ssDNA formed during strand exchange that do not enter the gel. Joint molecules (jm) are smaller branched ssDNA/dsDNA intermediates. RFIII is a linearized 5′-[^{32}P]-labeled M13mp18 dsDNA. The other substrate, circular M13mp18 ssDNA, is unlabeled and does not show on the phosphorimage. UvsX-wt, UvsX-H195A, and UvsX-H195Q proteins were used at a concentration of 6 μM (a) or 3 μM (b), respectively. Reactions in (b) also contained 1.43 μM Gp32. All reactions contained 10 μM [^{32}P]RFIII, and 10 μM ssDNA. ATP (final concentration, 3 mM) was used to initiate each reaction. An ATP-regenerating system consisting of 10 U ml^{-1} pyruvate kinase and 3.3 mM PEP was included in all reactions.

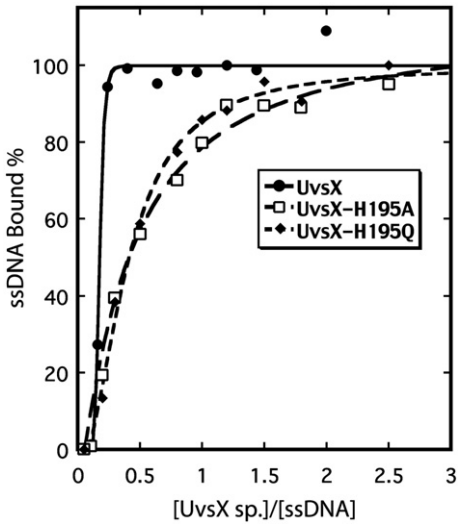

Fig. 3. Basal ssDNA-binding activities of UvsX wild type and mutants. Protein–ssDNA interactions were measured via an OliGreen dye-displacement assay, as described in Materials and Methods. OliGreen dye was stoichiometrically bound to 1 μM M13mp18 ssDNA in 20 mM Tris-acetate (pH 7.4), 1 mM DTT, and 50 mM NaCl, and then the mixture was titrated with wild-type UvsX (closed circles), UvsX-H195Q (open squares), or UvsX-H195A (closed diamonds) protein, while following the change in OliGreen fluorescence.

Kinetics of ssDNA-dependent ATP hydrolysis with ATP as variable substrate

The kinetics of the ssDNA-dependent ATPase activity of wild-type UvsX protein were investigated previously.[6] Here, we present the steady-state kinetic parameters of ATP hydrolysis by the UvsX-H195Q and UvsX-H195A mutants, in direct comparison with those of wild-type UvsX. Figure 4 shows typical time courses of ATP hydrolysis with nucleotide substrates/products resolved by thin-layer chromatography (TLC). The figure clearly illustrates the production of both ADP and AMP products by wild-type UvsX. In comparison, UvsX-H195Q and UvsX-H195A mutants produce ADP at a rate exceeding that of wild type under the conditions tested; however, their AMP production is strongly suppressed compared to that of wild type (Fig. 4).

To quantify differences in the ATPase properties of UvsX wild type and mutants, steady-state kinetic experiments were performed with ATP as variable substrate and at constant saturating ssDNA concentrations. Results are shown in Fig. 5 and Table 1. Reaction velocities were measured independently for ADP and AMP production using the TLC assay described under Materials and Methods. Velocity

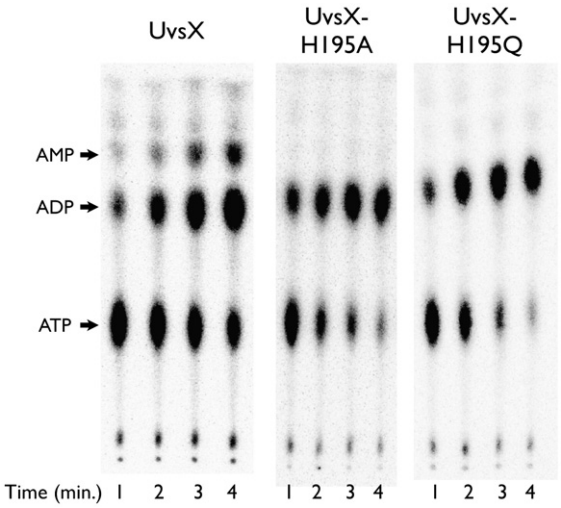

Fig. 4. Comparison of ssDNA-dependent ATPase reactions catalyzed by UvsX, UvsX-H195A, and UvsX-H195Q under maximum velocity conditions. TLC assays for ATP hydrolysis were performed as described in Materials and Methods. Chromatogram shows consumption of α-[^{32}P]ATP substrate and generation of labeled ADP and AMP products as a function of time. Reactions contained 0.45 μM wild-type or mutant UvsX protein as indicated, 3 mM α-[^{32}P]ATP, and either 10 μM (wild-type reactions) or 100 μM (mutant reactions) M13mp18 ssDNA.

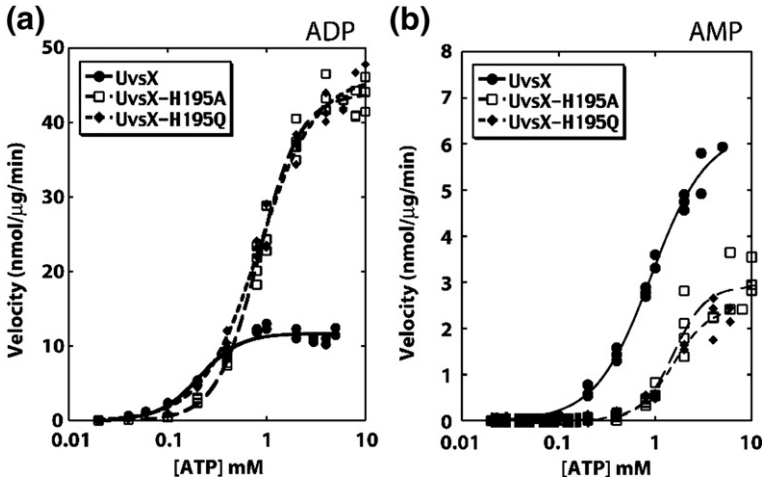

Fig. 5. Kinetics of ssDNA-dependent ATP hydrolysis by UvsX and mutants, with ATP as variable substrate. (a) Steady-state rates of ATP hydrolysis to ADP catalyzed by UvsX-wt (closed circles), UvsX-H195A (open squares), and UvsX-H195Q (closed diamonds). (b) Steady-state rates of ATP hydrolysis to AMP catalyzed by UvsX-wt (closed circles), UvsX-H195A (open squares), and UvsX-H195Q (closed diamonds). Note the expanded scale compared to (a). Reaction velocities were determined using TLC assays, as described in Materials and Methods. Data were fitted using the Hill equation (Eq. (1)).

curves are sigmoidal in nature (Fig. 5); therefore, data were analyzed by fitting either to the Hill equation or to the logistic sigmoid function.[29–32] Under apparent maximum velocity conditions (saturating ATP and ssDNA), wild-type UvsX exhibited a k_{cat} of 8.6 s^{-1} for ADP production *versus* a k_{cat} of 4.6 s^{-1} for AMP production (Table 1), for an ADP/AMP product ratio of ~1.9. These parameters are similar to those previously published.[6] In both reactions (ADP and AMP generation), wild-type UvsX exhibits strong positive homotropic cooperativity for the ATP substrate (Fig. 5 and Table 1). The apparent K_m values of wild-type UvsX for ATP are similar to previously published values.[6] With wild-type UvsX, the apparent K_m for ATP is ~4-fold lower, and k_{cat}/K_m is ~8-fold higher, when measured for the ADP-producing reaction *versus* the AMP-producing reaction (Table 1).

The two UvsX missense mutants H195A and H195Q are remarkably similar to each other in terms of their ATPase kinetics, but exhibit surprising differences from wild-type UvsX. Under apparent maximum velocity conditions (saturating ATP and ssDNA), both mutants exhibit ~4-fold increases in k_{cat} value for ADP production compared to wild type (Fig. 5 and Table 1). At the same time, both mutants show a 2- to 3-fold reduced k_{cat} for AMP production compared to wild-type UvsX (Table 1). Therefore, the ADP/AMP production ratio of the mutants is on the order of 15–19, or approximately 10-fold greater than the ratio observed for the wild-type enzyme. The cooperativity of ATP binding is maintained in both mutants; however, apparent K_m values for ATP are significantly higher for the two mutants compared to wild-type UvsX (Table 1). For both mutants, k_{cat}/K_m values for the ADP-producing reaction exceed those for the AMP-producing reaction by a factor of approximately 30 (Table 1). The data therefore indicate that UvsX-H195A and UvsX-H195Q mutants both have a markedly higher specificity than wild-type UvsX for generating ADP, instead of AMP, during ssDNA-dependent ATP hydrolysis.

Kinetics of ssDNA-dependent ATP hydrolysis, with ssDNA as variable cofactor

Results of experiments performed with ssDNA as variable component and at constant saturating ATP concentration are shown in Fig. 6 and Table 2. As expected, k_{cat} values are similar to those obtained in the ATP-variable experiments (Fig. 5 and Table 1). Wild-type UvsX exhibits interesting differences in the kinetics of ADP *versus* AMP production, as ssDNA is varied. The apparent K_m for ssDNA is 8-fold higher in the AMP-generating reaction than in the ADP-generating reaction (Table 2). Also, ADP production occurs with very high cooperativity towards ssDNA (Hill coefficient $h \approx 4$), whereas cooperativity towards ssDNA appears greatly reduced ($h \approx 1.3$) in the AMP-generating reaction. These results suggest that the ADP- and AMP-producing ATPase reactions may

Table 1. Steady-state kinetic parameters for ssDNA-dependent ATPase reactions of UvsX, UvsX-H195A, and UvsX-H195Q, with ATP as variable substrate

	UvsX		UvsX-H195A		UvsX-H195Q	
	ADP[a]	AMP[b]	ADP[a]	AMP[b]	ADP[a]	AMP[b]
k_{cat} (s^{-1})	8.57±0.21	4.61±0.21	32.19±0.62	2.14±0.13	33.87±0.99	1.82±0.14
$K_{m,ATP}$ (mM)	0.21±0.01	0.91±0.06	0.84±0.04	1.56±0.10	0.84±0.04	1.56±0.13
h[c]	2.11±0.21	1.50±0.09	2.04±0.12	2.62±0.42	1.51±0.09	2.31±0.31
k_{cat}/K_m (s^{-1} M^{-1})	4.1×10^4	5.1×10^3	3.8×10^4	1.4×10^3	4.0×10^4	1.2×10^3

Results were obtained from TLC ATPase assays by fitting that data to the Hill equation. Error is based on a minimum of three data sets.
[a] Apparent kinetic parameters associated with the production of ADP from ATPase reactions.
[b] Apparent kinetic parameters associated with the production of AMP from ATPase reactions.
[c] Hill parameter describing homotropic cooperativity for the ATP substrate.

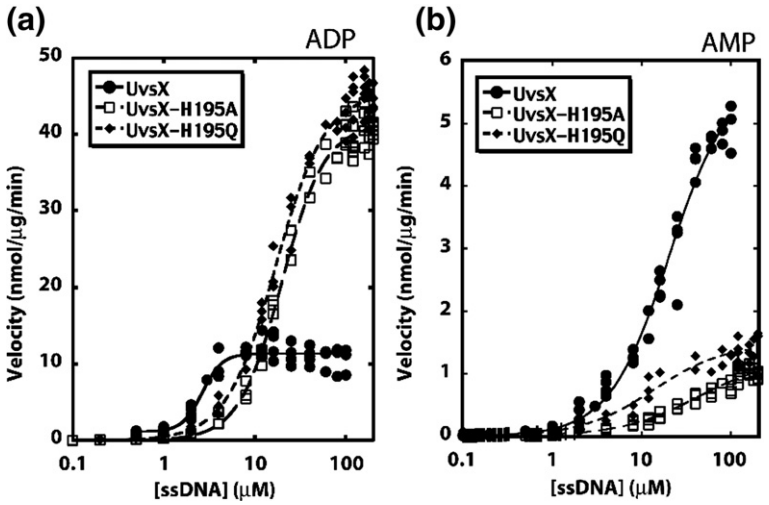

Fig. 6. Kinetics of ssDNA-dependent ATP hydrolysis by UvsX and mutants, with ssDNA as variable cofactor. (a) Steady-state rates of ATP hydrolysis to ADP catalyzed by UvsX-wt (closed circles), UvsX-H195A (open squares), and UvsX-H195Q (closed diamonds). The velocity-*versus*-ssDNA-concentration curve for UvsX-wt contains a minimal asymptote; thus, the data were fitted to the logistic sigmoid function (Eq. (3)). (b) Steady-state rates of ATP hydrolysis to AMP catalyzed by UvsX-wt (closed circles), UvsX-H195A (open squares), and UvsX-H195Q (closed diamonds). Note the expanded scale compared to (a). The data were fitted to either the Michaelis–Menten equation (Eq. (2)) for AMP production or the Hill equation (Eq. (1)) for ADP production.

differentially modulate the ssDNA-binding affinity/cooperativity of UvsX.

UvsX-H195A and UvsX-H195Q mutants both exhibit reduced cooperativity for ssDNA compared to wild-type UvsX (Fig. 6 and Table 2). In fact, with both mutants, the Hill coefficient is reduced to approximately 1 in the AMP-generating reaction, implying little or no cooperativity for ssDNA in this reaction component. UvsX-H195A and UvsX-H195Q exhibit significant differences in ssDNA-binding affinity compared to wild type and to each other (Table 2). H195Q's apparent K_m for ssDNA is 6-fold higher than that of wild type in the ADP-generating reaction, but its K_m in the AMP-generating reaction actually appears lower than that of wild type. In contrast, H195A's apparent K_m for ssDNA is 7-fold higher than that of wild type in the ADP-generating reaction, and its K_m in the AMP-generating reaction is 2-fold higher than that of wild type. Put in perspective, it takes 42.3 μM ssDNA to yield a half-maximal velocity of AMP production by H195A, *versus* only 2.7 μM ssDNA to yield a half-maximal velocity of ADP production by wild-type UvsX (Table 2).

The data in Table 2 indicate that UvsX-H195A is, overall, the weakest binder to ssDNA under steady-state conditions, whereas H195Q appears to retain intermediate ssDNA-binding affinity compared to H195A and wild type. Thus, steady-state ssDNA-binding affinity correlates closely with DNA strand-exchange activity. Based on studies at variable ssDNA concentrations, UvsX wild type, H195Q, and H195A exhibit a small range of k_{cat}/K_m values for ADP production, but a larger range of k_{cat}/K_m values for AMP production (Table 2). As a result, the k_{cat}/K_m ratios for the ADP-producing reactions *versus* the AMP-producing reactions increase from 15 (wild type) to 24 (H195Q) to 71 (H195A), indicating an increasing specificity for ADP over AMP production with loss of hydrogen-bonding capability at the allosteric switch position.

ADPase activities of UvsX and mutants

UvsX could produce AMP by directly hydrolyzing ATP to AMP plus pyrophosphate, or it could carry out a stepwise reaction, generating ADP plus phosphate in step 1, followed by AMP plus phosphate in step 2. To begin resolving between these models, we examined the abilities of UvsX wild type and mutants to carry out an ssDNA-dependent ADPase reaction. The reactions were slow and so were carried out over a 4-day time period to ensure that linearity was

Table 2. Steady-state kinetic parameters for ssDNA-dependent ATPase reactions of UvsX, UvsX-H195A, and UvsX-H195Q, with ssDNA as variable cofactor

	UvsX		UvsX-H195A		UvsX-H195Q	
	ADP[a,b]	AMP[b,c]	ADP[a,d]	AMP[c,e]	ADP[a,d]	AMP[c,e]
k_{cat} (s^{-1})	8.32±0.24	4.22±0.25	30.32±0.47	0.91±0.11	33.36±0.57	1.09±0.09
$K_{m,ssDNA}$ (μM)	2.66±0.19	20.35±1.90	19.78±0.66	42.26±10.39	16.96±0.67	13.63±2.96
h[f]	3.97±0.81	1.30±0.09	1.84±0.11	1	1.65±0.10	1
k_{cat}/K_m (s^{-1} M^{-1})	3.1×10^6	2.1×10^5	1.5×10^6	2.2×10^4	2.0×10^6	8.2×10^4

Results were obtained from TLC ATPase assays. Error is associated with a minimum of three experimental titrations.
[a] Apparent kinetic parameters associated with the production of ADP from ATPase reactions.
[b] Parameters and error obtained from fitting to the logistic sigmoid equation.
[c] Apparent kinetic parameters associated with the production of AMP from ATPase reactions.
[d] UvsX-H195A and UvsX-H195Q ADP data were fitted to the Hill equation.
[e] UvsX-H195A and UvsX-H195Q AMP data were both fitted to the Michaelis–Menten equation.
[f] Hill parameter describing cooperativity in ATP hydrolysis as a function of ssDNA concentration.

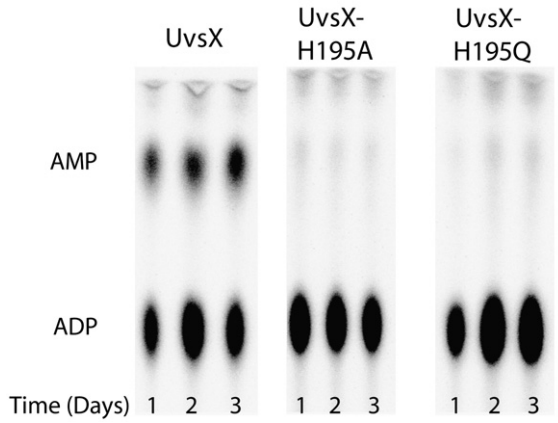

Fig. 7. Slow ADP hydrolysis by UvsX protein requires His195. TLC assays for ADP hydrolysis were performed as described in Materials and Methods. Chromatogram shows consumption of α-[^{32}P]ADP substrate and generation of labeled AMP product as a function of time. Reactions contained 0.45 μM wild-type or mutant UvsX protein as indicated, 40 μM ssDNA, and 20 mM ADP.

established. The TLC time courses in Fig. 7 show that significant hydrolysis of an exogenous ADP substrate to an AMP product occurs with wild-type UvsX; however, the k_{cat} of the reaction is only 6.3×10^{-5} s^{-1} (Table 3), which is 70,000-fold slower than the rate of AMP generation observed with ATP as starting substrate (Table 1). The apparent K_m of wild-type UvsX for exogenous ADP is ~14.5 mM (Table 3), which is 16-fold higher than the apparent K_m for ATP in the AMP-generating reaction (Table 1). These results indicate that the AMP produced in reactions starting with ATP as substrate does not arise through the rebinding of free ADP product to the enzyme, since free ADP is such a poor substrate. The apparent K_m values of wild-type UvsX for ssDNA are similar between the ADPase reaction and the AMP-generating component of the ATPase reaction (Tables 2 and 3).

Figure 7 also shows that the H195A and H195Q mutations effectively knock out UvsX's ADPase activity. The k_{cat} values of both are estimated to be approximately 4×10^{-8} s^{-1} (Table 3), which is barely distinguishable from background. This rate is 7–8 orders of magnitude slower than the rates of AMP production observed with UvsX-H195A and UvsX-H195Q in reactions starting with ATP as substrate (Table 1).

Pyrophosphate production by UvsX and mutants

Rates of inorganic pyrophosphate (PP_i) production by UvsX wild-type, H195A, and H195Q were measured during ssDNA-dependent ATPase reactions using the spectrophotometric coupled assay system described in Materials and Methods. Briefly, this assay measures PP_i production by coupling its consumption by PP_i:fructose-6-phosphate phosphotransferase to NADH oxidation catalyzed by glyceraldehyde-3-phosphate dehydrogenase, via linking reactions catalyzed by aldolase and triosephosphate isomerase. All three forms of UvsX exhibited slow rates of PP_i production (k_{cat} on the order of 0.03–0.05 s^{-1}; Table 3) compared to their rates of AMP production as measured in TLC assays (Tables 1 and 2). This amounted to an AMP/PP_i production ratio of ~150 for wild type and ~30 for both mutant forms of UvsX. Control experiments in which different amounts of exogenous PP_i were spiked into reaction mixtures confirmed that the coupled assay system had sufficient range to measure PP_i production rates equivalent to the fastest rates of ATP consumption observed in our experiments, plus sufficient sensitivity to measure much lower rates (data not shown). Our failure to detect significant PP_i production by UvsX conflicts with the stated findings of a previous study.[6] Our data suggest that AMP production via direct hydrolysis of ATP to AMP+PP_i is not an important component of the UvsX ATPase mechanism. Instead, the data in Table 3 argue that both wild-type and His195 missense mutant forms of UvsX prefer a processive stepwise pathway of AMP production in which: (1) ATP is first hydrolyzed to ADP+inorganic phosphate (P_i), and (2) ADP is retained in the active site and hydrolyzed to AMP+P_i before it can be released.

Discussion

Results of this study demonstrate that residue His195 plays major roles in regulating ssDNA binding, nucleotidase, and DNA strand-exchange properties of UvsX recombinase, consistent with its predicted roles in sensing the γ-phosphate of bound ATP and as an allosteric switch. The data also highlight striking differences in kinetic properties between UvsX and other RecA orthologs, which may

Table 3. Pyrophosphate and ADPase kinetics of UvsX-wt, UvsX-H195A, and UvsX-H195Q

		PP_i production[a]	ADPase[b]
UvsX	k_{cat} (s^{-1})	0.0304±0.007	$6.33\times10^{-5}\pm6.2\times10^{-7}$
	$K_{m,ADP}$ (mM)	ND	~14.5
	$K_{m,ssDNA}$ (μM)	ND	14.0±1.23
UvsX-H195A	k_{cat} (s^{-1})	0.0515±0.009	$\leq4\times10^{-8}$
UvsX-H195Q	k_{cat} (s^{-1})	0.0508±0.027	$\leq4\times10^{-8}$

[a] Pyrophosphate production levels during ATP hydrolysis were determined by spectrophotometric coupled assay.
[b] Kinetic parameters of AMP production using ADP as direct substrate. Reaction rates were calculated from a minimum of five different reactions. $K_{m,ADP}$ and $K_{m,ssDNA}$ for UvsX-H195A and UvsX-H195Q were not determined for PP_i production and ADPase activities.

be useful for understanding the evolution of catalytic and allosteric mechanisms in the RecA/Rad51 family.

UvsX exhibits much greater tolerance for mutations at His195 than does *E. coli* RecA at its equivalent position, Gln194. UvsX-H195Q represents a conservative mutation that, in principle, should make the active site more RecA-like. In fact, this mutant retains weak DNA strand-exchange activity that is stimulated further by Gp32. In addition, both UvsX-H195Q and UvsX-H195A mutants are stronger ssDNA-dependent ATPases than wild-type UvsX. Both observations stand in contrast with EcRecA, in which the reciprocal mutation Q194H and also Q194A both knock out RecA recombination/repair and LexA coprotease functions *in vivo*, while *in vitro* studies of RecA-Q194A demonstrated loss of both strand-exchange and ssDNA-dependent ATPase activities.[17] Thus, UvsX appears to have a more flexible active site that can accommodate structural changes while still maintaining ssDNA-activated enzymatic activities.

Based on kinetic parameters of ssDNA-dependent ATP hydrolysis and on equilibrium binding experiments, both UvsX-H195A and UvsX-H195Q mutants exhibit lower apparent binding affinity and cooperativity for ssDNA than does wild-type UvsX. This is consistent with the notion that His195 plays a key role in inducing a high-affinity ssDNA-binding conformation of UvsX in response to ATP binding. The steady-state data indicate that UvsX-H195A has the weakest ssDNA-binding affinity, while that of H195Q is intermediate between H195A and wild type. The dramatic reduction in the apparent cooperativity of ssDNA binding seen with H195A and H195Q (Table 2) strongly implicates the His195 residue as a transmitter of allosteric effects between UvsX protomers in the presynaptic filament.

Details of the kinetics of ADP and AMP production via the ssDNA-dependent ATPase reaction indicate that UvsX-ssDNA filaments contain two different asymmetric classes of active sites—one that generates ADP, and another that generates AMP (possible models shown in Fig. 8). Recall that the ADP- and AMP-producing reactions occur simultaneously in reaction mixtures containing UvsX, MgATP, and ssDNA. The steady-state kinetic parameters of the ADP- and AMP-producing reactions can therefore be measured in the same experiment under identical conditions (Figs. 4–6). The results demonstrate that, for wild-type UvsX, the apparent K_m and k_{cat}/K_m values for the ATP substrate are markedly different in ADP-producing *versus* AMP-producing reactions (Table 1). Even more dramatic differences are seen in the K_m and k_{cat}/K_m values for the ssDNA substrate; in addition, the Hill coefficient for ssDNA is reduced from ~4 in the ADP-producing reaction to only 1.3 in the AMP-producing reaction (Table 2). Thus, the simultaneous reactions exhibit distinct kinetic properties with respect to both ATP and ssDNA binding. This argues strongly for two classes of active sites within UvsX-ssDNA presynaptic filaments. Evidence also exists for active-site asymmetry in other members

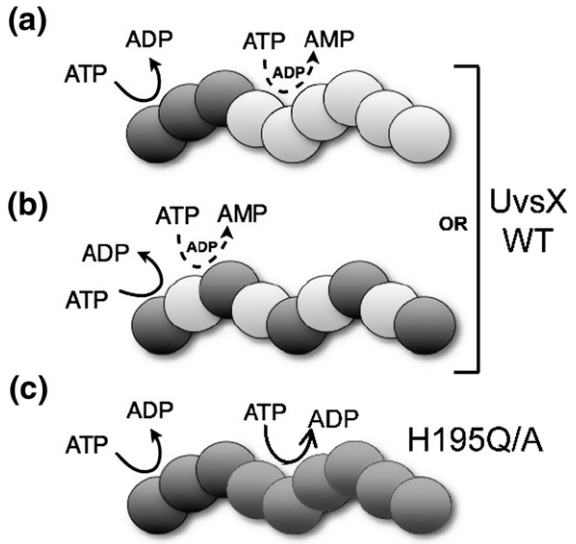

Fig. 8. Hypothetical models for active-site asymmetry within the UvsX-ssDNA presynaptic filament. Filaments are proposed to contain two different classes of ATPase active sites—one generating ADP, and another generating AMP. Shown here are two possible active-site arrangements for wild-type UvsX in which (a) active sites differ at filament ends *versus* interior subunits (e.g., as shown with ADP generated from active sites near filament ends and AMP generated from active sites in the filament interior), or (b) ADP and AMP generation occurs at alternating active sites along the filament (e.g., at alternating protomer–protomer interfaces). In both models (a and b), AMP-producing sites do so by a sequential mechanism without ADP release. (c) Mutations at residue His195 decrease active-site asymmetry and reduce AMP production by UvsX, possibly by enhancing the rate of ADP release. See Discussion for details.

of the RecA family, including ScRad51 and EcRecA: The X-ray crystallographic structure of ScRad51 filaments formed in the presence of ssDNA and nucleoside triphosphate revealed that alternating protomers are in different conformations, creating two classes of nucleotide-binding sites at alternating protomer–protomer interfaces within the filament.[33] A related "dimeric protomer" model was proposed to explain the existence of two classes of NTP-binding sites within presynaptic filaments of EcRecA protein.[34] Therefore, conformations containing asymmetric active sites may be a general feature of the dynamics of presynaptic filaments from many organisms, with T4 UvsX representing an extreme example in which the asymmetry is reflected not only in substrate binding but also in catalysis.

How might the two different classes of active sites be distributed within filaments? UvsX-ssDNA filaments have head, tail, and interior regions, with most association/dissociation events occurring at the head or the tail. Conceivably, UvsX could assume different conformations at the head or tail region *versus* the filament interior,[35] forming different classes of active sites that regionally produce either ADP or AMP as products of the ATPase reaction (Fig. 8a). Another possible arrangement is the alternating-protomers

configuration observed crystallographically for ScRad51.[33] If this model also holds for UvsX, then conceivably it could produce ADP and AMP at alternating sites along the filament (Fig. 8b). A third possibility that cannot be strictly ruled out yet is that each UvsX protomer contains two ATPase active sites (not shown), as evidence was presented for two nucleotide-binding sites in each protomer of *M. smegmatis* RecA protein.[14]

Results of this study suggest that within the asymmetric UvsX-ssDNA filament, sites that generate AMP do so by a stepwise kinetic mechanism, wherein ATP is first hydrolyzed to ADP + P_i then ADP is retained at the active site and further hydrolyzed to AMP + P_i. Thus, while all active sites generate ADP, only one class of sites releases ADP as product, while the second class retains it and performs additional chemistry. Evidence for the stepwise mechanism includes the extremely low observed rates of hydrolysis of exogenous ADP by UvsX, as well as the very low observed ratio of PP_i/AMP product formation (Table 3). Our data conflict with a previous report stating that UvsX produces AMP and PP_i in approximately equal quantities (unpublished results mentioned in Formosa and Alberts[6]). We considered the possibility that our purified UvsX fraction contained a contaminating pyrophosphatase activity. Control reactions argued against this possibility, since identical rates of PP_i consumption were observed in the presence and in the absence of UvsX when known amounts of exogenous PP_i were added to the coupled assay system (data not shown). We are unaware of any other enzyme that generates AMP from ATP by a processive stepwise mechanism. Further experimentation will be necessary to confirm this mechanism for UvsX.

It is clear that His195 plays an important role in maintaining active-site asymmetry and thereby promoting the AMP-producing component of UvsX's ATPase reaction. The H195A and H195Q mutations decrease active-site asymmetry, as indicated by a ~10-fold increase in ADP/AMP product ratio compared to wild type, based on the k_{cat} values in Tables 1 and 2. Simultaneously, the k_{cat} of ADP production increases by ~4-fold over wild type in H195Q/A mutants (Tables 1 and 2). The combined data suggest that both mutations increase the rate of ADP product release. We hypothesize that UvsX-H195Q/A mutants release ADP too quickly to undergo a subsequent conformational change that locks the filament into its asymmetric form. Rapid ADP release by these mutants may reset filaments to a "ground state" having predominantly one class of active sites, as shown in the model in Fig. 8c. Such filaments would primarily generate ADP as product, which is what we observe experimentally. The relationship between ADP retention/release and conformational changes within presynaptic filaments is an attractive target for further biochemical and mutagenesis studies.

Diminished AMP production by the UvsX-H195Q mutant correlates strongly with diminished DNA strand-exchange activity, suggesting that active-site asymmetry maintained by His195 is important for UvsX recombination function. (UvsX-H195A lacks any strand-exchange activity, indicating that the reaction has been completely uncoupled from ATPase activity in this mutant.) AMP production by UvsX is associated with relatively low ssDNA-binding affinity and cooperativity, as inferred from kinetic parameters in Table 2. This suggests a potential biological function for AMP production in the turnover and dynamics of UvsX-ssDNA presynaptic filaments. Previous work demonstrated that T4 presynaptic filaments undergo assembly and collapse, which are closely linked to the ATPase cycle.[37] AMP production by UvsX may help to ensure that filaments eventually dissociate from DNA, clearing the way for replication enzymes that are needed for recombination-dependent replication/repair. Similarly, by lowering UvsX cooperativity, AMP production may promote the breakup of long filaments by increasing the probability of interior subunit dissociation. Recent studies have demonstrated that presynaptic filament turnover is an important component of DNA strand-exchange reactions promoted by RecA family recombinases.[35–37] AMP production by UvsX may be one mechanism by which the T4 recombination system ensures efficient turnover of recombination intermediates.

Materials and Methods

Reagents, enzymes, and nucleic acids

Chemicals, biochemicals, and commercial enzymes were purchased from Sigma, unless specifically noted. [α-^{32}P]ATP was purchased from Amersham Biosciences. Polyethyleneimine cellulose chromatography plates were purchased from EMD Chemicals. Restriction endonucleases were purchased from New England Biolabs. Oligonucleotide primers were purchased from Qiagen. Circular ssDNA from the bacteriophage M13mp18 was isolated by extraction from purified phage particles.[38] Supercoiled M13mp18 dsDNA (RFI) was purchased from New England Biolabs. Linearized RFIII M13mp18 dsDNA was generated by digestion with XbaI, treated with calf intestinal phosphatase to dephosphorylate the 5′ ends, and radiolabeled using T4 polynucleotide kinase in accordance with the manufacturer's instructions. The radiolabeled RFIII was further purified by Qiagen's gel extraction protocol. All DNA concentrations were determined by absorbance at 260 nm and are reported in units of nucleotides.

T4 Gp32 and UvsX proteins

Gp32 (34 kDa) and wild-type UvsX (43 kDa) proteins were purified and stored as described.[24,39] All T4 protein stock solutions used in this study were judged to be greater than 98% pure, based on analyses of Coomassie-blue-stained SDS polyacrylamide gels. In addition, all protein solutions were found to be nuclease-free according to published criteria.[40] All protein concentrations were determined by absorbance at 280 nm, using molar extinction coefficients of 69,760 $(M\ cm)^{-1}$ for UvsX and 41,360 $(M\ cm)^{-1}$ for Gp32 (unpublished results).[41]

Site-directed mutagenesis of UvsX

Plasmid pET27b(+)-encoding UvsX was a generous gift from Dr. S. J. Benkovic (Pennsylvania State University). The H195A and H195Q mutants were created using the QuikChange site-directed mutagenesis kit (Stratagene). Primers were designed by creating a missense mutation at positions 583–585 in the UvsX gene, changing the codon sequence of CAT to GCA for UvsX-H195A, and to CAA for UvsX-H195Q. To construct UvsX-H195A, primer 1 (5′-CCATGTATTGCTATTAACGCAACATACGAAA-CACAAGAAATGTTTAG-3′) and reverse complement primer 2 (5′-CTAAACATTTCTTGTGTTTCGTATG-TTGCGTTAATAGCAATACATGG-3′) were used. For UvsX-H195Q, primer 3 (5′-CCATGTATTGCTATTAAC-CAAACATACGAAACACAAGAAATGTTTAG-3′) and reverse complement primer 4 (5′-CTAAACATTTCTTG-TGTTTCGTATGTTGGTTAATAGCAATACATGG-3′) were used. Plasmids pET27b-UvsX-H195A and pET27b-UvsX-H195Q were sequenced at the Vermont Cancer Center to verify successful mutagenesis. These plasmids were transformed into *E. coli* BL21(DE3) cells. Growth and induction were carried out at 37 °C in LB media containing 75 μg ml^{-1} kanamycin. Recombinant proteins were induced by the addition of 1 mM IPTG for 4 h. Subsequent purification, storage, and quantification of UvsX-H195A and UvsX-H195Q proteins were carried out as described for wild-type UvsX.[24]

DNA strand-exchange assay

DNA strand-exchange reactions were carried out at 37 °C as described,[6] with the following adjustments. The reaction mixtures contained 20 mM Tris-acetate (pH 7.4), 90 mM potassium acetate, 10 mM magnesium acetate, 1 mM DTT, 100 μg ml^{-1} BSA, 10 U ml^{-1} pyruvate kinase, 3.3 mM phosphoenolpyruvate, 10 μM M13mp18 ssDNA, 10 μM linear M13mp18 dsDNA (RFIII), 0 or 1 μM Gp32, and 0.5–6 μM recombinase, depending on the experiment. Reaction mixtures were incubated at 37 °C for 5 min and initiated by the addition of ATP to a final concentration of 3 mM. The reaction was allowed to continue for the time stated and stopped by the addition of strand-exchange Stop solution [final concentrations: 1× Promega loading dye, 5% SDS, and 40 mM ethylenediaminetetraacetic acid (EDTA)]. The samples (10 μl) were separated by electrophoresis at 130 V for 2 h through 1% agarose gels in the presence of a Tris-acetate–EDTA buffer system. The gels were dried onto Millipore Immobilon-Ny^+ using a gel drier overnight at 45 °C and exposed to a K-screen (Kodak) for 1 day. The phosphorimage was then scanned using a Bio-Rad Personal Molecular Imager-FX and analyzed using Quantity One V4.5.1 (Bio-Rad) software.

ssDNA-binding assays

Protein–ssDNA interactions of wild-type and mutant UvsX proteins were quantified by OliGreen dye displacement. OliGreen dye (Molecular Probes/Invitrogen) undergoes great fluorescence enhancement upon saturation with ssDNA. Protein binding to ssDNA reduces OliGreen fluorescence by displacing the dye from the polynucleotide. Fluorescence measurements were made on a PTI Quantamaster QM-6 fluorometer, with excitation and emission wavelengths set at 480 and 520 nm, respectively. Dye-displacement assays were carried out at 25 °C in buffer containing 20 mM Tris-acetate (pH 7.4), 1 mM DTT, 10 mM $MgCl_2$, and 50 mM NaCl. The concentration of M13mp8 ssDNA was 1 μM nucleotides. The amount of OliGreen dye added was stoichiometric with respect to ssDNA. This amount was determined empirically from the break point of calibration curves in which dye was titrated into a fixed concentration of ssDNA while dye fluorescence was being measured. Experimental dye/ssDNA solutions were titrated with UvsX, UvsX-H195Q, or UvsX-H195A protein while the decrease in dye fluorescence was being monitored. Parallel control experiments included: (1) titration of identical dye/ssDNA solutions with equivalent volumes of UvsX storage buffer, and (2) titration of dye solution lacking ssDNA with protein. Control data were used to correct experimental data for small effects of dilution, photobleaching, and dye–protein interactions.

ATPase assays

Rates of ssDNA-dependent ATP hydrolysis by wild-type and mutant UvsX proteins were determined by TLC assays. Reactions were performed at 37 °C as described,[6] except for the following changes. Unless otherwise stated, the reactions contained 20 mM Tris-acetate (pH 7.4), 10 mM magnesium acetate, 90 mM potassium acetate, 1 mM DTT, 100 μg ml^{-1} BSA, 0.45 μM wild-type or mutant UvsX recombinase, 0–120 μM M13mp18 ssDNA, and 0–10 mM ATP, in a final reaction volume of 100 μl. In experiments with ssDNA as variable component, reactions were initiated by the addition of ATP to a final concentration of 3 mM ([α-^{32}P] ATP final specific activity, 10 μCi ml^{-1}). In experiments with ATP as variable component, enzyme concentrations were lowered to 0.1 μM to maximize linear reaction time points, and ssDNA concentration was fixed at 20 μM (UvsX wild-type reactions) or 100 μM (UvsX mutant reactions). At various time points, 5-μl samples were removed and quenched into 2 μl of 280 mM EDTA to give a final concentration of 80 mM EDTA. Quenched samples were spotted out at 0.5-μl volumes onto polyethyleneimine cellulose TLC plates (20 cm×20 cm) at 1-cm intervals. After all the samples had been spotted and dried, the TLC plates were developed with 0.75 M KH_2PO_4 and air-dried. The TLC plates were exposed for 1 h to a K-screen (Kodak) and scanned by a Bio-Rad Personal Molecular Imager-FX. Quantification of the phosphorimage was performed by Quantity One v. 4.5.1 (Bio-Rad) software and subsequently fitted using KaleidaGraph v. 3.6.2 (Synergy Software) software. Except as noted below, kinetics data were fitted to the Hill equation:

$$v = \frac{V_{\max}[S]^h}{K_{0.5}^h + [S]^h} \quad (1)$$

where v is the initial velocity at any given substrate concentration S, $V_{\max}$ is the maximum velocity, $K_{0.5}$ is the apparent Michaelis constant (equal to the substrate concentration at which $v = 0.5V_{\max}$), and h is the Hill coefficient. For UvsX-H195A and UvsX-H195Q mutants, rates of AMP production at variable ssDNA concentrations were best described by the Michaelis–Menten equation:

$$v = \frac{V_{\max}[S]}{K_m + [S]} \quad (2)$$

where K_m is the Michaelis constant. For UvsX wild type, rates of ADP production at variable ssDNA concentrations were best described by the logistic sigmoid function:

$$\frac{v}{[S]^h} = v_{\min} + \frac{V_{\max} - V_{\min}}{1 + \exp(-k(x - X_{50}))} \quad (3)$$

where V_{min} is the minimum velocity associated with basal levels of hydrolysis, k is proportional to the Hill coefficient [$k=h\ln(10)$], x is the logarithmic cofactor concentration (ssDNA), and X_{50} is the negative logarithm of apparent K_m. The logistic sigmoid function is mathematically equivalent to the Hill equation, but incorporates an additional minimal asymptote parameter to explain basal levels of activity.[29–32] A minimum of three reactions were run at each substrate concentration, and velocities were corrected for the amount of recombinase in each reaction.

ADPase assays

ADPase reaction rates were determined using the standard TLC conditions described above, except that ADP, instead of ATP, was used as substrate. [α-^{32}P]ADP was generated by reacting 25 μM [α-^{32}P]ATP with 0.75 U ml^{-1} hexokinase in 5 mM Hepes (pH 7.6), 30 mM $MgCl_2$, and 300 μM D-glucose, as described previously.[42] The reaction was allowed to proceed for 4 h at 30 °C and immediately stopped by boiling for 3 min. The radiolabeled ADP was determined to contain 1.66% unreacted [α-^{32}P]ATP based on TLC separation and densitometry using QuantityOne Software (Bio-Rad). The final reactions mixtures contained 20 mM ADP ([α-^{32}P]ADP final specific activity, 10 μCi ml^{-1}) and were carried out for 4 days at 20 °C. Reaction rates were determined as described above for ATPase TLC assays.

Pyrophosphate assay

Pyrophosphate production rates by UvsX wild type, UvsX-H195A, and UvsX-H195Q were determined by modification of a published coupled assay system described in Van Schaftingen *et al.*[43] Reactions contained 0.45 μM recombinase, 4.5 μM ssDNA (for UvsX wild type) or 40 μM ssDNA (for UvsX mutants), 17 mM glucose 6-phosphate, 2.5 mM fructose 6-phosphate, 1 μM fructose-2,6-bisphosphate, 0.46 mM NADH, 2.86 U ml^{-1} aldolase, 2.86 U ml^{-1} glyceraldehyde-3-phosphate dehydrogenase, 2.86 U ml^{-1} triosephosphate isomerase, and 0.043 U ml^{-1} pyrophosphate:fructose-6-phosphate phosphotransferase. Reactions were carried out in 20 mM Tris-acetate (pH 7.4), 10 mM magnesium acetate, and 90 mM potassium acetate buffer containing 6 U ml^{-1} PK and 3 mM PEP for regeneration of ATP from ADP. Reactions were carried out at 37 °C in a volume of 350 μl. Reactions were started by the addition of 5 mM ATP. Reactions were monitored using a Hitachi U-2000 spectrophotometer, recording change in A_{380} over time. Rates were calculated from the linear portions of time courses. All reactions were repeated a minimum of five times. Pyrophosphate-positive controls were performed as described above by adding an initial concentration of 2.5 mM pyrophosphate. Spiking of the recombinase reactions with 2.5 μM and 2.5 mM pyrophosphate during the reaction course was performed for additional positive controls.

Sequence alignments

Multiple amino acid sequence alignments were performed using Tcoffee software,[44] using full-length protein sequences obtained from the National Center for Biotechnology Information (NCBI) and Protein Data Bank (PDB) protein databases. Sequences used in the alignment included the following: enterobacteria phage T4 UvsX (NCBI AAD42669), *D. radiodurans* RecA (NCBI BAA21330), *M. tuberculosis* RecA (PDB 1MO6), *Mycobacterium segmatis* RecA (PDB 1UBG), *E. coli* RecA (NCBI AAA75588), *Prochlorococcus* phage P-SSM2 (cyanophage) UvsX (NCBI AAX44563), *Prochlorococcus* phage P-SSM4 (cyanophage) UvsX (NCBI AAX46948), enterobacteria phage RB49 UvsX (NCBI AAL87837), enterobacteria phage RB69 UvsX (NCBI AAP75946), *Pyrococcus furiosus* RadA (NCBI AAL82050), *Thermoplasma acidophilum* RadA (NCBI NP_394563), *Mus musculus* Rad51 (NCBI BAA02718), *Homo sapiens* Rad51 (NCBI AAD49705), *S. cerevisiae* Rad51 (NCBI CAA45563), *T. parva* strain Muguga Rad51 (NCBI XP_763865), *H. sapiens* Dmc1 (NCBI CAG30372), and *T. parva* strain Muguga Dmc1 (NCBI XP_76380).

Acknowledgements

The authors thank Dr. Hang Xu, Dr. Jie Liu, and Jennifer Tomczak for helpful comments, suggestions, and technical assistance.

This work was supported by National Institutes of Health program project grant P01 CA098993.

References

1. Shibata, T. (2001). Functions of homologous DNA recombination. *RIKEN*, **41**, 21–23.
2. Bianco, P. R., Tracy, R. B. & Kowalczykowski, S. C. (1998). DNA strand exchange proteins: a biochemical and physical comparison. *Front. Biosci.* **3**, D570–D603.
3. Beernink, H. T. & Morrical, S. W. (1999). RMPs: recombination/replication mediator proteins. *Trends Biochem. Sci.* **24**, 385–389.
4. Bleuit, J. S., Xu, H., Ma, Y., Wang, T., Liu, J. & Morrical, S. W. (2001). Mediator proteins orchestrate enzyme–ssDNA assembly during T4 recombination-dependent DNA replication and repair. *Proc. Natl Acad. Sci. USA*, **98**, 8298–8305.
5. Kreuzer, K. N. (2000). Recombination-dependent DNA replication in phage T4. *Trends Biochem. Sci.* **25**, 165–173.
6. Formosa, T. & Alberts, B. M. (1986). Purification and characterization of the T4 bacteriophage uvsX protein. *J. Biol. Chem.* **261**, 6107–6118.
7. Story, R. M., Bishop, D. K., Kleckner, N. & Steitz, T. A. (1993). Structural relationship of bacterial RecA proteins to recombination proteins from bacteriophage T4 and yeast. *Science*, **259**, 1892–1896.
8. Story, R. M. & Steitz, T. A. (1992). Structure of the recA protein–ADP complex. *Nature*, **355**, 374–376.
9. Akiba, T., Ishii, N., Rashid, N., Morikawa, M., Imanaka, T. & Harata, K. (2005). Structure of RadB recombinase from a hyperthermophilic archaeon, *Thermococcus kodakaraensis* KOD1: an implication for the formation of a near-7-fold helical assembly. *Nucleic Acids Res.* **33**, 3412–3423.
10. Qian, X., Wu, Y., He, Y. & Luo, Y. (2005). Crystal structure of *Methanococcus voltae* RadA in complex with ADP: hydrolysis-induced conformational change. *Biochemistry*, **44**, 13753–13761.
11. Xing, X. & Bell, C. E. (2004). Crystal structures of *Escherichia coli* RecA in a compressed helical filament. *J. Mol. Biol.* **342**, 1471–1485.
12. Rajan, R. & Bell, C. E. (2004). Crystal structure of RecA from *Deinococcus radiodurans*: insights into the structural basis of extreme radioresistance. *J. Mol. Biol.* **344**, 951–963.

13. Datta, S., Ganesh, N., Chandra, N. R., Muniyappa, K. & Vijayan, M. (2003). Structural studies on MtRecA–nucleotide complexes: insights into DNA and nucleotide binding and the structural signature of NTP recognition. *Proteins*, **50**, 474–485.
14. Krishna, R., Manjunath, G. P., Kumar, P., Surolia, A., Chandra, N. R., Muniyappa, K. & Vijayan, M. (2006). Crystallographic identification of an ordered C-terminal domain and a second nucleotide-binding site in RecA: new insights into allostery. *Nucleic Acids Res.* **34**, 2186–2195.
15. Chen, Z., Yang, H. & Pavletich, N. P. (2008). Mechanism of homologous recombination from the RecA–ssDNA/dsDNA structures. *Nature*, **453**, 214–489.
16. Xing, X. & Bell, C. E. (2004). Crystal Structures of *Escherichia coli* RecA in complex with MgADP and MnAMP-PNP. *Biochemistry*, **43**, 16142–16152.
17. Kelley, J. A. & Knight, K. L. (1997). Allosteric regulation of RecA protein function is mediated by Gln194. *J. Biol. Chem.* **272**, 25778–25782.
18. Hortnagel, K., Voloshin, O. N., Kinal, H. H., Ma, N., Schaffer-Judge, C. & Camerini-Otero, R. D. (1999). Saturation mutagenesis of the *E. coli* RecA loop L2 homologous DNA pairing region reveals residues essential for recombination and recombinational repair. *J. Mol. Biol.* **286**, 1097–1106.
19. Voloshin, O. N., Wang, L. & Camerini-Otero, R. D. (2000). The homologous pairing domain of RecA also mediates the allosteric regulation of DNA binding and ATP hydrolysis: a remarkable concentration of functional residues. *J. Mol. Biol.* **303**, 709–720.
20. Menetski, J. P. & Kowalczykowski, S. C. (1985). Interaction of recA protein with single-stranded DNA. Quantitative aspects of binding affinity modulation by nucleotide cofactors. *J. Mol. Biol.* **181**, 281–295.
21. Bleuit, J. S., Ma, Y., Munro, J. & Morrical, S. W. (2004). Mutations in a conserved motif inhibit single-stranded DNA binding and recombination mediator activities of bacteriophage T4 UvsY protein. *J. Biol. Chem.* **279**, 6077–6086.
22. Hinton, D. M. & Nossal, N. G. (1986). Cloning of the Bacteriophage T4 uvsX gene and purification and characterization of the T4 uvsX recombination protein. *J. Biol. Chem.* **261**, 5663–5673.
23. Yonesaki, T. & Minagawa, T. (1989). Synergistic action of three recombination gene products of bacteriophage T4, uvsX, uvsY, and gene 32 proteins. *J. Biol. Chem.* **264**, 7814–7820.
24. Ando, R. A. & Morrical, S. W. (1998). Single-stranded DNA binding properties of the UvsX recombinase of bacteriophage T4: binding parameters and effects of nucleotides. *J. Mol. Biol.* **283**, 785–796.
25. Kodadek, T., Wong, M. L. & Alberts, B. M. (1988). The mechanism of homologous DNA strand exchange catalyzed by the Bacteriophage T4 uvsX and gene 32 proteins. *J. Biol. Chem.* **263**, 9427–9436.
26. Yassa, D. S., Chou, K. M. & Morrical, S. W. (1997). Characterization of an amino-terminal fragment of the bacteriophage T4 uvsY recombination protein. *Biochimie*, **79**, 275–285.
27. Kowalczykowski, S. C., Lonberg, N., Newport, J. W., Paul, L. S. & von Hippel, P. H. (1980). On the thermodynamics and kinetics of the cooperative binding of bacteriophage T4-coded gene 32 (helix destabilizing) protein to nucleic acid lattices. *Biophys. J.* **32**, 403–418.
28. Scheerhagen, M. A., Vlaanderen, C. A., Blok, J. & van Grondelle, R. (1986). Binding stoichiometry of the gene 32 protein of phage T4 in the complex with single stranded DNA deduced from boundary sedimentation. *J. Biomol. Struct. Dyn.* **3**, 887–898.
29. Hill, A. V. (1910). The possible effects of the aggregation of the molecules of haemoglobin on its oxygen dissociation curve. *J. Physiol. (Lond.)* **40**, *4–7*.
30. Tikunova, S. B., Rall, J. A. & Davis, J. P. (2002). Effect of hydrophobic residue substitutions with glutamine on Ca(2+) binding and exchange with the N-domain of troponin C. *Biochemistry*, **41**, 6697–6705.
31. Black, D. J., Tikunova, S. B., Johnson, J. D. & Davis, J. P. (2000). Acid pairs increase the N-terminal Ca^{2+} affinity of CaM by increasing the rate of Ca^{2+} association. *Biochemistry*, **39**, 13831–13837.
32. George, S. E., Su, Z., Fan, D., Wang, S. & Johnson, J. D. (1996). The fourth EF-hand of calmodulin and its helix–loop–helix components: impact on calcium binding and enzyme activation. *Biochemistry*, **35**, 8307–8313.
33. Conway, A. B., Lynch, T. W., Zhang, Y., Fortin, G. S., Fung, C. W., Symington, L. S. & Rice, P. A. (2004). Crystal structure of a Rad51 filament. *Nat. Struct. Mol. Biol.* **11**, 791–796.
34. Lauder, S. D. & Kowalczykowski, S. C. (1991). Asymmetry in the recA protein–DNA filament. *J. Biol. Chem.* **266**, 5450–5458.
35. Liu, J., Qian, N. & Morrical, S. W. (2006). Dynamics of bacteriophage T4 presynaptic filament assembly from extrinsic fluorescence measurements of GP32–SSDNA interactions. *J. Biol. Chem.*
36. Krejci, L., Van Komen, S., Li, Y., Villemain, J., Reddy, M. S., Klein, H. *et al.* (2003). DNA helicase Srs2 disrupts the Rad51 presynaptic filament. *Nature*, **423**, 305–309.
37. Symington, L. S. & Heyer, W. D. (2006). Some disassembly required: role of DNA translocases in the disruption of recombination intermediates and dead-end complexes. *Genes Dev.* **20**, 2479–2486.
38. Sambrook, J., Fritsch, E. F. & Maniatis, T. (1989). Molecular Cloning: A Laboratory Manual, 2nd edit Cold Spring Harbor Laboratory Press, Plainview, NY.
39. Ishmael, F. T., Alley, S. C. & Benkovic, S. J. (2001). Identification and mapping of protein–protein interactions between gp32 and gp59 by cross-linking. *J. Biol. Chem.* **276**, 25236–25242.
40. Sweezy, M. A. & Morrical, S. W. (1997). Single-stranded DNA binding properties of the uvsY recombination protein of bacteriophage T4. *J. Biol. Chem.* **266**, 927–938.
41. Gill, S. C. & von Hippel, P. H. (1989). Calculation of protein extinction coefficients from amino acid sequence data. *Anal. Biochem.* **182**, 319–326.
42. Stefan, C., Stalmans, W. & Bollen, M. (1996). Threonine autophosphorylation and nucleotidylation of the hepatic membrane protein PC-1. *Eur. J. Biochem.* **241**, 338–342.
43. Van Schaftingen, E., Lederer, B., Bartrons, R. & Hers, H. G. (1982). A kinetic study of pyrophosphate: fructose-6-phosphate phosphotransferase from potato tubers. Application to a microassay of fructose 2,6-bisphosphate. *Eur. J. Biochem.* **129**, 191–195.
44. Poirot, O., O'Toole, E. & Notredame, C. (2003). Tcoffee@igs: a web server for computing, evaluating and combining multiple sequence alignments. *Nucleic Acids Res.* **31**, 3503–3506.